Dislocation theory-based cohesive model for microstructurally short fatigue crack growth

Shardul Panwar, Veera Sundararaghavan*

Department of Aerospace Engineering, University of Michigan, Ann Arbor, MI, 48109, USA

ABSTRACT

A continuous representation of dislocations is used to represent a mode-II crack and the associated plastic zone. In the original formulation of dislocation theory, the friction stress that opposes the motion of the dislocations is represented by a constant stress. In our new formulation, we embed a cohesive zone in the plastic region in front of a crack tip by representing the friction stress as a function of the crack displacement. This allows cohesive zone models (obtainable from a lower scale simulation, such as molecular dynamics) to be integrated into a dislocation theory-based model, for the first time, to predict short crack growth. The details of this new formulation are shown for the two cases: the crack and the associated plastic zone inside a grain, and the crack and the associated plastic zone tip at the grain boundary. The main features of this new model are discussed along with an experimental comparison to the case of microstructurally short fatigue crack growth across two grains in a Ni-based CMSX-4 alloy.

Introduction

In the last couple of decades, the area of short fatigue crack growth has generated a lot of interest. This is due to the availability of modern experimental techniques, such as X-ray Tomography and Focused Ion Beam (FIB), that have facilitated deeper investigation into this area and a growing realization that the fatigue life of some materials may depend entirely on the short fatigue crack growth regime [1]. According to Newman et al. [2], short fatigue cracks can be classified into two categories: microstructurally short cracks and physically short cracks (PSC). A crack is called microstructurally short when its length is on the order of the microstructural size, such as a grain diameter, whereas, it is called physically short when the crack length is larger than a few grain diameters.

Traditionally, linear elastic fracture mechanics (LEFM) has been used to quantify the fatigue crack growth rate in materials. However, in the short fatigue crack growth regime, LEFM suffers from several limitations, such as: (1) the observed fatigue crack growth in a specimen is much faster than that calculated from LEFM, (2) the observed fatigue crack growth can happen at stress intensity factors much lower than the threshold stress intensity factor predicted by LEFM, and (3) the local microstructure of the material can negatively affect the fatigue crack growth rate and, in some cases, arrest the crack growth. There are various models that have been proposed in recent years to overcome

these limitations. Some models are based on a modified LEFM approach, such as Newman's crack closure model [2,3], while others are based on the explicit incorporation of microstructural features, such as grain boundaries and precipitates, and their interactions with the crack tip. Christ et al. [1] have classified these later type of models into three categories: (1) empirically-based models that are informed and driven by experiments [4], (2) mechanism-based models, such as the Bilby-Cottrell-Swinden (BCS) model [5], the Taira-Tanaka-Nakai model [6,7], the Navarro-Rios model [8–11], and (3) models based on discrete dislocations [12]. The mechanism-based models find their origin in the work of Bilby et al. [5]. The BCS model follows on the work of Head and Louat [13] and approximates the crack and the associated plastic zone by a continuous distribution of dislocations. In the BCS model, Bilby et al. [5] derived the plastic zone length for a macroscopic crack in an infinite domain and showed that their plastic zone expression is similar to the expression presented by Dugdale [14]. Barenblatt [15] has also proposed a similar expression for the plastic zone length. The models developed by Barenblatt [15] and Dugdale [14] form the basis of cohesive zone models. Willis [16] has shown that if the cohesive surface energy density is equal to the fracture toughness, then LEFM and Barenblatt theory are equivalent. In a computational framework, Hillerborg et al. [17] have utilized the cohesive zone model to describe the damage behavior of concrete. For quasi-brittle materials, Planas et al. [18] have shown the various generalizations, including initiation

criteria and the extension to mixed mode failure [19] and specializations, including size effects and the asymptotic behavior of the cohesive zone models. Cohesive zone models have also been used to study failure process in other materials, such as ceramics [20], polymers [21,22], and ductile metals [23]. A good overview of the application of cohesive zone models to the materials previously mentioned is given by Elices et al. [24]. In cohesive zone models, the fracture process is represented as a gradual process of separation between two material surfaces [25]. Thus, the separation process is represented in a phenomenological form by the relationship between the surface traction and the distance between the two surfaces. This process is similar to a softening process that occurs at the front of a crack tip. On the other hand, Weertman [26] has modified the BCS model to include the effect of work hardening at the fatigue crack tip by relating the average stress in the plastic zone in front of the crack tip to the crack tip displacement. He assumed this relationship to be a power law with two parameters. In the Taira-Tanaka-Nakai model, the BCS model is applied to the case of slip bands emanating from a crack tip inside a grain; Taira et al. [6] recognized that, when a plastic tip reaches a grain boundary, the dislocations pile up against the grain boundary. Using Muskhelishvili's inversion formula [27], they solved a two-dimensional dislocation density equation with the plastic tip blocked by a grain boundary by assuming that, mathematically, dislocation density becomes infinite at a grain boundary. They refer to this as an unbounded solution; conversely, the original BCS model employs a bounded solution. Tanaka et al. [7] have extended the Taira-Tanaka-Nakai model by including the crack closure for stage II cracks and calculating the fatigue crack growth rates across stage I and stage II. Later, Navarro and De Los Rios (N-R) [8–11] combined both the bounded and unbounded solutions into a general expression for the dislocation distribution. In addition, they applied a critical grain boundary strength parameter that a crack needs to overcome in order to propagate into the next grain. To examine the statistics of the short fatigue crack growth in textured FCC polycrystals, Wilkinson [28,29] used the N-R model within the Monte Carlo framework.

In this paper, the new contribution is integration of a cohesive zone model (such as [14,15]) within the BCS [5] and the Taira-Tanaka-Nakai [6] models to simulate microstructurally short fatigue crack growth through multiple grains. The BCS and Taira-Tanaka-Nakai models assume that the friction stress opposing the dislocation motion is the local yield stress of the material. Similarly, for a macroscopic crack, Dugdale's model assumes that the cohesive stress opposing the opening of a Mode-I crack tip is the yield stress of the material. However, molecular dynamics (MD) simulations have shown that the cohesive strength varies with the crack opening displacement [30], and, in the shear mode, it is closely approximated by an exponential relationship [31]. We assume that the friction stress opposing the dislocation motion is a function of the crack displacement, as is shown by MD simulations. Incorporating this assumption in the BCS and Taira-Tanaka-Nakai models, we derive an expression for the bounded and unbounded solutions to the dislocation density distribution equations. These expressions are solved numerically to get the crack displacement and the crack tip stress field.

The paper has been divided into four sections. Section 1 gives an introduction of the BCS and Taira-Tanaka-Nakai formulations. Section 2 details our new formulation that combines the cohesive zone model with first the BCS model and then the Taira-Tanaka-Nakai model. We call this new formulation the Cohesive-BCS model. As has been done in Taira et al. [6], this new formulation is extended to fatigue in Section 3. In Section 4, the new features of this model are compared to those of the BCS and Taira-Tanaka-Nakai models. Finally, the new formulation is utilized in the prediction of microstructurally short fatigue crack growth rates in a Ni-based CMSX-4 specimen and results are compared to experiments [32].
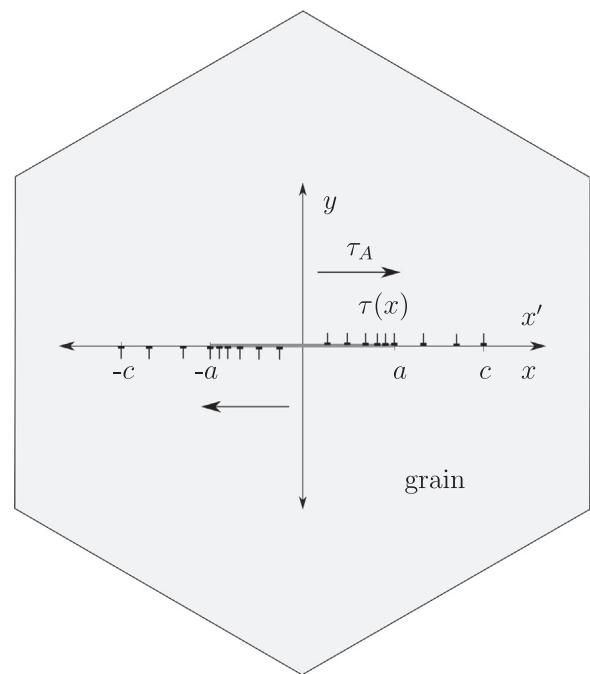
Fig. 1. Dislocation distribution under an applied shear stress τ_A.

1. The BCS and Taira-Tanaka-Nakai models

Based on the theory of continuously distributed dislocations [13], Bilby et al. [5] have derived the dislocation density expression for a uniformly stressed solid containing a notch with a plastic zone in the front. This is called a bounded solution, since the dislocation density is bounded at the plastic tip. Taira et al. [6] have derived the dislocation density expression for a slip band that is blocked at a grain boundary and is emanating from a crack tip. This solution is referred to as an unbounded solution, since the dislocation density is unbounded at the plastic tip due to the dislocation pile up. Both of these solutions are employed to calculate the microstructurally short fatigue crack growth rate across multiple grains by assuming that the crack growth rate is proportional to the crack tip displacement [8]. Using this assumption, the bounded solution gives the crack growth rate when the crack and the associated plastic zone are inside a grain (Fig. 1), while the unbounded solution gives the crack growth rate when the plastic zone is blocked by a grain boundary (Fig. 2).

This section is structured in two parts: Part I describes the important expressions for the bounded solution of the dislocation density, and Part II shows the dislocation distribution expression for the unbounded solution and the expression for the stress distribution in front of the plastic tip blocked by a grain boundary.

1.1. Part I: The bounded solution from the BCS model

In the BCS model, the plastic zone in front of the crack tip is simplified by assuming that it is in the same plane as the crack plane (Fig. 1). Within the plastic zone, the friction stress $\tau_f(x)$ that resists the dislocation motion is assumed to be equal to the yield stress. The crack faces are considered to be traction free. The crack tip in this paper is always at $x = \pm a$, $y = 0$, while the plastic tip is always at $x = \pm c$, $y = 0$.

The dislocation distribution that exists on the traction free crack plane $(-a < x < a)$ has a stress associated with it. This stress $\tau(x)$ should be in equilibrium with the applied stress. Thus,
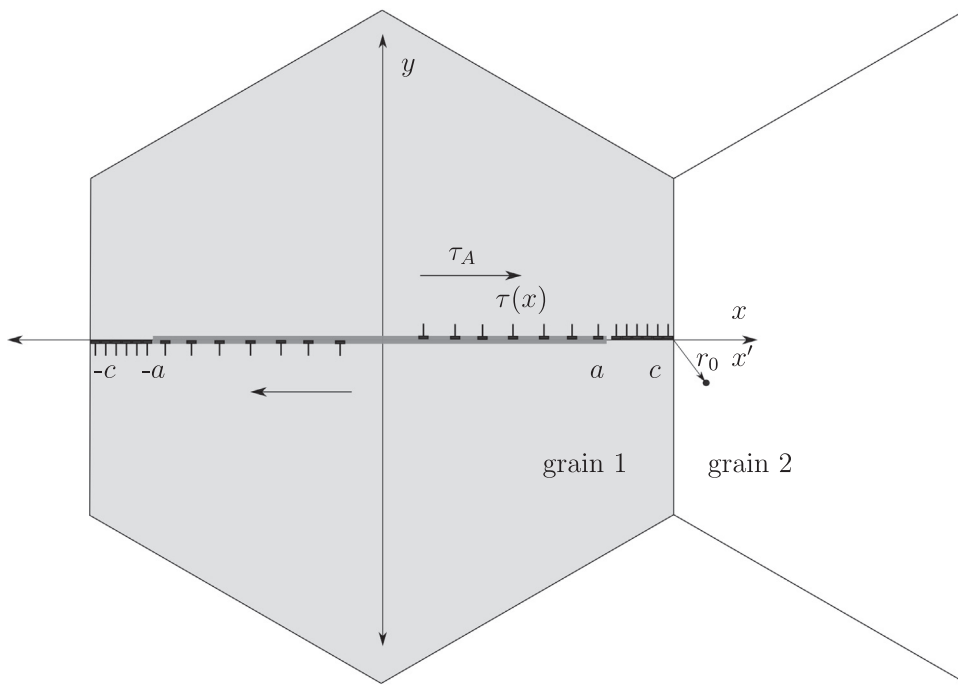
$$\tau(x) + \tau_A = 0$$
$$\tau(x) = -\tau_A \tag{1.1}$$

Moreover, the stress $\tau(x)$ produced by the dislocation distribution inside the plastic zone ($a < |x| < c$) is resisted by the friction stress $\tau_f(x)$. This resistance should be in equilibrium with the applied stress τ_A. Thus,

$$\tau_f(x) - \tau(x) = \tau_A$$
$$\tau(x) = \tau_f(x) - \tau_A \tag{1.2}$$

In Fig. 1, the shear stress at x due to the presence of a dislocation at x' is given by

$$\tau(x) = \frac{G}{2\pi\alpha} \int_{-c}^{c} \frac{B(x')}{x - x'} dx', \quad -c < x < c \tag{1.3}$$

The above expression (Eq. (1.3)) is solved for the dislocation density $B(x)$ by Muskhelishvili's inversion formula [27]. The final expression is

$$B(x) = -\frac{2\alpha\sqrt{c^2 - x^2}}{\pi G} \int_{-c}^{c} \frac{\tau(x')}{(x - x')\sqrt{c^2 - x'^2}} dx', \quad -c < x < c \tag{1.4}$$

and the condition for the dislocation density $B(x)$ to be bounded at $x = \pm c$ is given by

$$\int_{-c}^{c} \frac{\tau(x)}{\sqrt{c^2 - x^2}} dx = 0 \tag{1.5}$$

In the above expressions (Eqs. (1.4) and (1.5)), c represents the half length of the crack and the associated plastic zone, G is the shear modulus, $\alpha = 1$ for screw dislocation, $\alpha = 1 - \nu$ for edge dislocation, and ν is the Poisson's ratio. In general, c must also satisfy another condition [33], given by

$$\int_{-c}^{c} \frac{x\tau(x)}{\sqrt{c^2 - x^2}} dx = \frac{Gb_T}{2\alpha} \tag{1.6}$$

Here, $b_T = b_R + b_L$ is the net Burgers vector of all the dislocations, b_R is the net Burgers vector of the dislocations in the positive x direction, $0 < x < \infty$, and b_L is the net Burgers vector of the dislocations in the negative x direction, $-\infty < x < 0$. If $\tau(x)$ is a symmetric function of x, then $b_T = 0$ and Eq. (1.6) is satisfied by symmetry, regardless of the value of c.

Eq. (1.4) contains a singular kernel and is solved in the Cauchy principal value sense. Eq. (1.5) is called the existence condition, and it determines the length of the plastic zone ($c - a$).

1.2. Part II: The unbounded solution from the Taira-Tanaka-Nakai model

Taira et al. [6] found that the BCS model can be used in the analysis of crystallographic slip bands emanating from the crack tip. They showed that, when these slip bands are on the order of the grain size, they can be influenced by a grain boundary (Fig. 2). To incorporate the interaction of the grain boundary with the dislocations, Eq. (1.3) is solved considering the dislocation density function to be unbounded at the plastic tip [27]. This adds an additional term to Eq. (1.4), and the final equation becomes

$$B(x) = -\frac{2\alpha\sqrt{c^2 - x^2}}{\pi G} \int_{-c}^{c} \frac{\tau(x')}{(x - x')\sqrt{c^2 - x'^2}} dx'$$
$$- \frac{2\alpha}{\pi G} \frac{x}{\sqrt{c^2 - x^2}} \int_{-c}^{c} \frac{\tau(x')}{\sqrt{c^2 - x'^2}} dx', \quad -c < x < c \tag{1.7}$$

Here,

$$\tau(x') = -\tau_A, \quad |x'| < a$$
$$\tau(x') = \tau_f(x') - \tau_A, \quad a < |x'| < c$$

The additional term in Eq. (1.7) is a delta-type function; a repulsive stress field, rising suddenly from zero to infinity, locks the leading dislocation. The integrand is the same as in the existence condition, Eq. (1.5), while the coefficient $\frac{x}{\sqrt{c^2 - x^2}}$ makes the dislocation density infinite at the grain boundary, $x = \pm c$. The length of the plastic zone is calculated from the grain size.

A stress ($S(r_0)$) at a point that is at a distance r_0 away from the grain boundary on the grain 2 slip plane (Fig. 2) is given in [13] by

$$S(r_0) = \frac{Gb}{2\pi\alpha} \int_{-c}^{c} \frac{B(x)}{x' - x} dx + \tau_A, \quad x' = c + r_0, \quad |x'| > c \tag{1.8}$$

where b is the burgers vector.

For both the models, the dislocation density $B(x)$ is related to the crack sliding displacement $D(x)$ by

$$B(x) = -\frac{dD(x)}{dx} \tag{1.9}$$
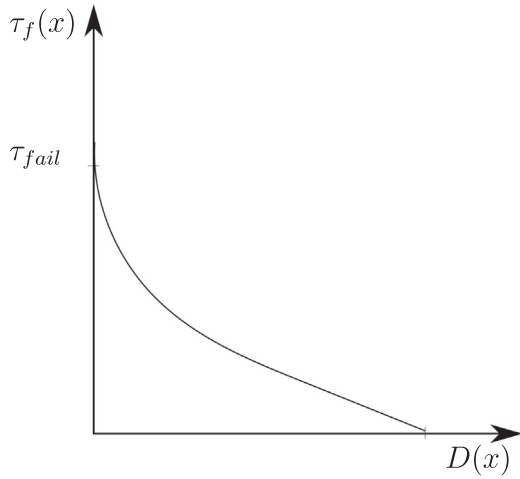
Fig. 3. Shear exponential traction-separation law.

2. Dislocation-based cohesive model (Cohesive-BCS model)

2.1. Cohesive model

The central theme of the cohesive theory of fracture is the representation of the fracture process as a gradual separation of the fracture surfaces. This is achieved through the use of numerous functional relationships between the fracture surface traction and the surface displacement. These relationships are called traction-separation laws. In literature, most of the traction-separation laws that have been developed are phenomenological [25]. In this paper, we also utilize an exponential relationship (Fig. 3) between the surface traction and the crack surface displacement [31].

$$\tau_f(x) = \tau_{fail} \exp(-h_s |D(x)|), \quad h_s > 0 \tag{2.1}$$

h_s in the above equation is a fitting parameter with units of L^{-1}. For monotonic failure, τ_{fail} is the slip system critical resolved shear stress. For fatigue failure, the value of τ_{fail} is lower than the critical resolved shear stress value, and this value is calibrated from experiments. Thus, the area under this curve (Fig. 3) represents the fracture energy of the slip system.

Putting Eq. (2.1) into Eq. (1.9) and integrating both sides from c to x gives

$$\ln(\tau_{fail}) - \ln(\tau_f(x)) = h_s \int_x^c B(x) dx, \quad a < |x| < c \tag{2.2}$$

The assumption used in the above equation is that the value of the stress at the plastic tip is equal to the critical resolved shear stress τ_{fail} of that slip system.

2.2. Bounded solution with a cohesive zone

The bounded solution of Eq. (1.4) is modified using Eq. (2.2), resulting in

$$\ln(\tau_{fail}) - \ln(\tau_f(x)) =$$
$$h_s \int_x^c \left(-\frac{2\alpha\sqrt{c^2-x^2}}{\pi G} \int_{-c}^c \frac{\tau(x')}{(x-x')\sqrt{c^2-x'^2}} dx' \right) dx, \quad a < |x| < c \tag{2.3}$$

This equation is a nonlinear Fredholm integro-differential equation of the second kind with a weakly singular kernel. The above expression is simplified using Eqs. (1.5) and (1.6). The procedure is described in detail in Appendix A. The final forms of Eq. (2.3) and Eq. (1.5) are shown below:

$$\ln(\tau_f(x)) = \frac{2h_s\alpha}{\pi G}\left(\int_a^c \tau_f(x') I_b dx'\right) + \ln(\tau_{fail}),$$
$$a < |x| < c \tag{2.4}$$

$$\int_a^c \frac{\tau_f(x)}{\sqrt{c^2-x^2}} dx = \frac{\pi\tau_A}{2} \tag{2.5}$$

Here,

$$I_b = \ln\left|\frac{x\sqrt{c^2-x'^2} + x'\sqrt{c^2-x^2}}{x\sqrt{c^2-x'^2} - x'\sqrt{c^2-x^2}}\right| + \ln\left|\frac{\sqrt{c^2-x'^2} + \sqrt{c^2-x^2}}{\sqrt{c^2-x'^2} - \sqrt{c^2-x^2}}\right|$$
$$- 2\frac{\sqrt{c^2-x^2}}{\sqrt{c^2-x'^2}}$$

These coupled equations (Eqs. (2.4) and (2.5)) are numerically solved for $\tau_f(x)$ and c using the Newton-Raphson scheme with a piecewise polynomial collocation method [34]. The latter method is described in detail in Appendix C.

2.3. Unbounded solution with a cohesive zone

Putting Eq. (1.7) into Eq. (2.2) again gives a nonlinear Fredholm integro-differential equation of the second kind. This expression is simplified using the symmetry of the stress function ($\tau(x)$). The final expression becomes

$$\ln(\tau_f(x)) = \frac{2h_s\alpha}{\pi G}\left(\int_a^c \tau_f(x') I_u dx'\right) - \frac{2h_s\alpha\tau_A}{G}\sqrt{c^2-x^2}$$
$$+ \ln(\tau_{fail}), a < |x| < c \tag{2.6}$$

Here, I_u is given by

$$I_u = \ln\left|\frac{x\sqrt{c^2-x'^2} + x'\sqrt{c^2-x^2}}{x\sqrt{c^2-x'^2} - x'\sqrt{c^2-x^2}}\right| + \ln\left|\frac{\sqrt{c^2-x'^2} + \sqrt{c^2-x^2}}{\sqrt{c^2-x'^2} - \sqrt{c^2-x^2}}\right|$$
$$- 2\left(\frac{\pi}{2} - \arcsin\frac{x}{c}\right)\frac{x'}{\sqrt{c^2-x'^2}}$$

The details of the above simplification are given in Appendix B.

There is no analytical method for calculating $\tau_f(x)$ from Eq. (2.5) or $S(r_0)$ from Eq. (1.14). Thus, we again employ a set of numerical schemes to solve these equations. These numerical schemes are described in Appendix C. Once $\tau_f(x)$ is found, the crack sliding displacement $D(x)$ is calculated from Eq. (2.1) and $S(r_0)$ is calculated from Eq. (1.14). The crack sliding displacement at the crack tip is the crack tip sliding displacement $D(a)$.

3. Fatigue crack growth

Under cyclic loading, the applied resolved shear stress τ_A varies between a maximum value τ_{max} and a minimum value τ_{min}. Assuming there is no crack extension between each complete cycle and no crack closure, the monotonic quantities in Eqs. (2.4), (2.5) and (2.6) are converted to cyclic quantities through the following transposition [6,26,28]:

$$\tau_A \rightarrow \Delta\tau_A = \tau_{max} - \tau_{min} = (1-R)\tau_{max}$$
$$\tau_f(x) \rightarrow 2\tau_f(x) \tag{3.1}$$

Here, R is the load ratio. For a polycrystalline specimen under a far field unaxial cyclic stress $\Delta\sigma$ (shown in Fig. 4), the local resolved cyclic shear stress $\Delta\tau_A^i$ on a slip plane i with the Schmid factor m_i is calculated using the Schmid single slip model to be

$$\Delta\tau_A^i = m_i\Delta\sigma = m_i(1 - R)\sigma_{max} \tag{3.2}$$

where m_i is the local Schmid factor of an active slip system and σ_{max} is the maximum value of the applied stress. The crack growth rate is calculated by assuming that it is proportional to the crack tip sliding displacement. Thus, an equation similar to the Paris law is obtained.

$$\frac{da}{dN} = \lambda D(a)^n \tag{3.3}$$

This assumption has been used in numerous analytical fatigue crack growth models [7,8,10,26,28]. The parameter λ is interpreted as a slip irreversibility factor with values between 0 (completely reversible) and
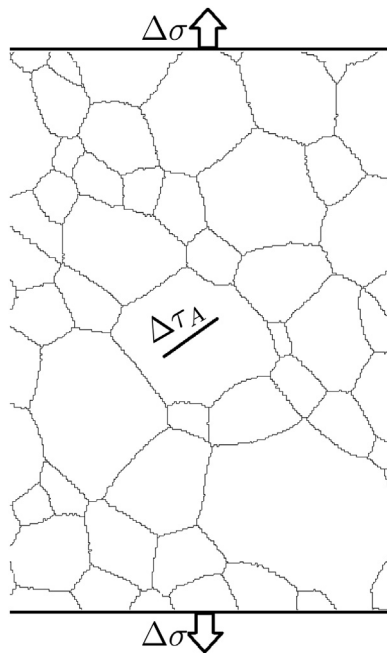
Fig. 4. Applied cyclic stress $\Delta\sigma$ resolved to a single slip shear stress $\Delta\tau_A$.

1 (completely irreversible). The parameter n describes the contributions from different crack displacement modes (I, II, III) on the crack tip sliding displacement $D(a)$.

4. Discussion

In this section, we highlight the differences between our Cohesive-BCS model and the BCS and Taira-Tanaka-Nakai models. The first part of the discussion section shows the effect of the cohesive parameter h_s on the dislocation stress and the crack sliding displacement. In the second part of the discussion section, we calibrate our model with data from experiments on Ni-based CMSX-4 alloy. This calibrated model is then used to predict microstructurally short fatigue crack growth across multiple grains in this alloy.

4.1. Comparison of the Cohesive-BCS model with the BCS and Taira-Tanaka-Nakai models

In this subsection, we study the impact of the cohesive parameter h_s on the dislocation stress and the crack sliding displacement. Using the values mentioned in Table 1, we solve for both the bounded and unbounded solutions of the Cohesive-BCS model (Section 2) for different values of parameter h_s. The BCS and Taira-Tanaka-Nakai solutions are also plotted in each figure to highlight the differences.

In Fig. 5, we plot the normalized dislocation stress ($\tau(x)/\tau_{fail}$) inside of and in front of the plastic zone. The dislocation stress at the tip of the crack ($x/a = 1$) reduces as we increase h_s. This is expected, as increasing h_s reduces the area under the traction-separation curve (Fig. 3), which reduces the fracture energy required to create a crack. This causes a higher number of dislocations to be emitted by the crack tip. Therefore,

Table 1
Material properties for a sensitivity study.

Variable	Values	Units
$\frac{G}{2\pi(1-\nu)}$	3776	GPa
σ	85	GPa
τ_{fail}	55	GPa
m_s	0.45	
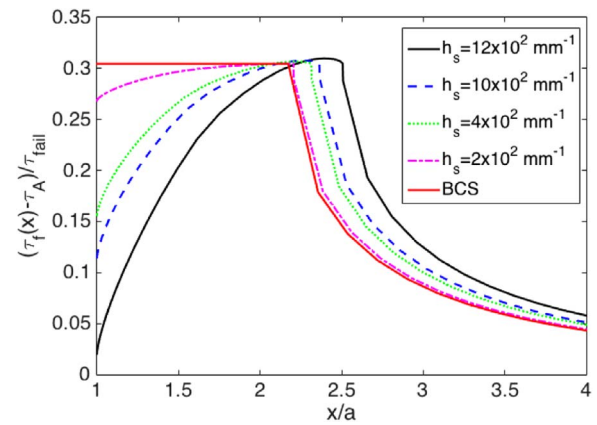
Fig. 5. The effect of h_s on the dislocation stress when the crack and the associated plastic zone are inside a grain.

increasing h_s reduces the dislocation stress. The friction stress at the crack tip ($\tau_f(a)$) reduces as h_s increases, which results in the increased mobility of the dislocations. This increased dislocation mobility causes the length of the plastic zone (c-a) to increase. In Fig. 5, the half length of the crack and the associated plastic zone c is shown to increase from $2.17a$ for $h_s = 1 \times 10^2 \, mm^{-1}$ to $2.53a$ for $h_s = 12 \times 10^2 \, mm^{-1}$. As we reduce h_s, the solution given by our model eventually converges to the BCS solution, since the exponential term in Eq. (2.1) goes to zero.

In Fig. 6, we plot the normalized crack sliding displacement against the distance from the crack tip ($x = a$) to the plastic tip ($x = c$). As previously stated, increasing h_s increases the number of dislocations that are emitted by the crack tip. This increased dislocation density at the crack tip increases the crack tip sliding displacement ($D(a)$). However, the increase in the number of dislocations also increases the length of the plastic zone ($c - a$). The overall effect of increasing h_s is distributed between the crack sliding displacement and the plastic zone length; therefore, the change in each of these quantities appears less significant than the increase in h_s.

In Fig. 7, the normalized dislocation stress ($(S(x) - \tau_A)/\tau_{fail}$) at the grain boundary ($x = c = \frac{D_g}{2}$) is plotted against the distance from the grain boundary in the adjacent grain (see Fig. 2). The dislocation stress increases as h_s increases. This is due to the increase in the number of dislocations emitted by the crack tip. These increased dislocations pile up at the grain boundary, causing the stress at the grain boundary to increase. Therefore, through the cohesive parameter h_s, we can also control the interaction between the crack plane and the grain boundary.

In Fig. 8, the value of c is constant and is equal to half of the grain

Fig. 6. The effect of h_s on the crack sliding displacement when the crack and the associated plastic zone are inside a grain.
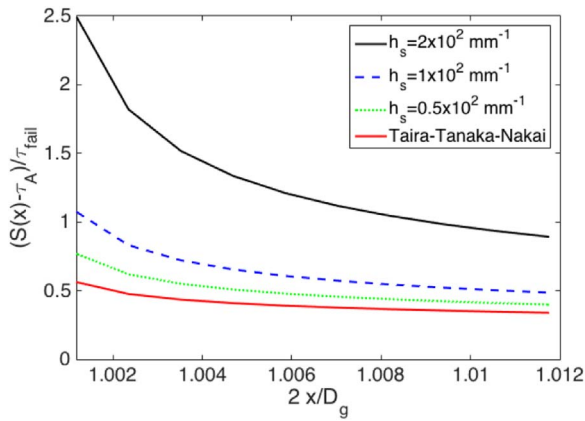
Fig. 7. The effect of h_s on the dislocation stress when the tip of the crack and the associated plastic zone is at the grain boundary. D_g is the grain size.
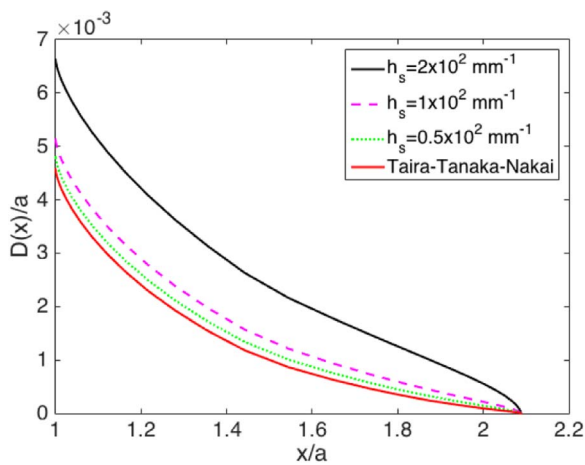
Fig. 8. The effect of h_s on the crack sliding displacement when the tip of the crack and the associated plastic zone is at the grain boundary.

size ($\frac{D_g}{2}$). As previously stated, increasing h_s increases the number of dislocations emitted by the crack tip. However, as compared to the case of the plastic zone being within the grain, the impact of increasing h_s is more prominent on the crack sliding displacement.

4.2. Microstructurally short fatigue cracks in a Ni-based CMSX-4 alloy

In this subsection, we utilize our Cohesive-BCS model to predict the growth of microstructurally short fatigue cracks in a Ni-based CMSX-4 alloy. To achieve this, we use the experiments performed by Marx et al. [32,35] and the equations described in Sections 2 and 3.

Marx et at. performed experiments on a single crystal and polycrystalline modification of a Ni-based CMSX-4 alloy [32]. The material properties of this alloy are given in Table 2.

To predict the microstructurally short fatigue crack growth behavior of this alloy, we calibrate the unknown slip system parameters (τ_{fail} and h_s) and the crack growth rate parameter (n) with the experiments. The

Table 2
Ni-based CMSX-4 alloy material properties

Variable	Value	Unit	Reference
G	72.27	GPa	[36]
ν	0.39		
α	$1 - \nu$		
τ_{crss}	363	MPa	[36]
σ_{max}	545	MPa	[32]
R	$- 0.1$		[32]
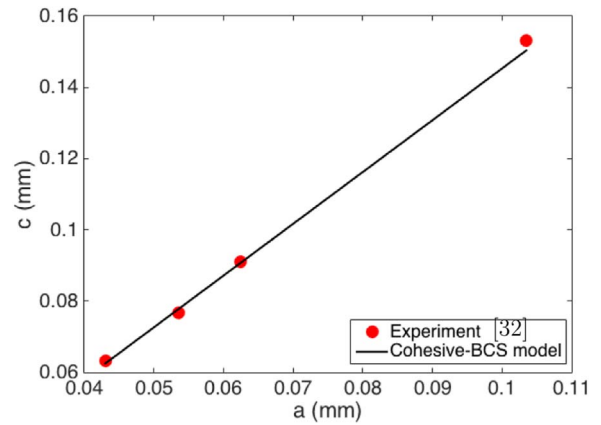
Fig. 9. Calibration of the cohesive parameters τ_{fail} and h_s from the experiments [32].

main difference between our new Cohesive-BCS model (described in Section 2) and the BCS model utilized in Marx et al. [35] is the elimination of the slip irreversibility parameter λ. The value of this parameter determines the reversibility of the dislocation emission process at the crack tip [35]. By embedding a cohesive zone in front of the crack tip we can control how many dislocations are emitted from the crack tip. The result of this procedure can be seen in Figs. 6 and 8; at the crack tip ($x/a = 1$), the value of the normalized crack tip sliding displacement ($D(a)/a$) changes with different values of the cohesive parameter h_s.

To calibrate the slip system parameters τ_{fail} and h_s to the experimental results, we use the plastic zone lengths measured from the Marx et al. experiments [32]. The preferred slip system for this FCC alloy is $\{111\} < 110>$.

In Fig. 9, the half lengths of the crack and the associated plastic zone were measured for cracks that were sufficiently far from the grain boundary. Here, we utilize Eqs. (2.4), (2.5), (3.1), and (3.2) and the material properties mentioned in Table 2 to calculate the values of c corresponding to various half crack lengths (a). We minimize the error between the experimentally calculated values and the numerically calculated values of c to calibrate the cohesive parameters. Thus, the calibrated values are

$$\tau_{fail} = 261.4 \ MPa$$
$$h_s = 10 \ mm^{-1}$$

The τ_{fail} value is similar to the BCS model τ_f value (263 MPa) mentioned in Marx et al. [35].

The next step in the calibration process is to determine the microstructurally short fatigue crack growth parameter n. This parameter is used to determine the relationship between the crack growth rate and the crack tip sliding displacement. We again solve the equations discussed in Sections 2.2 and 3 to determine the values of the crack tip sliding displacement ($D(x = a)$) corresponding to each half crack length (a). In Fig. 10, the experimental crack growth rates are plotted against the numerically determined crack tip sliding displacements. The nonlinear least square function in MATLAB [37] is then used to determine the value of the parameter n; $n = 1.411$ is the value that gives the best fit.

All the parameters, τ_{fail}, h_s, and n, have now been determined. We now utilize these parameters to predict the microstructurally short fatigue crack growth rates across multiple grains. The effect of a grain boundary on the crack has to be taken into account in order to understand the crack growth across multiple grains. The presence of a grain boundary can have a significant effect on crack growth. For example, the grain boundary can cause the crack growth rate to reduce or the crack growth to stop, depending on its features. However, in this paper, we have not modeled all the features of the grain boundary. As in [32], we use just one parameter, called the grain boundary critical stress intensity factor (ΔK_{gb}), the value of which is mentioned in
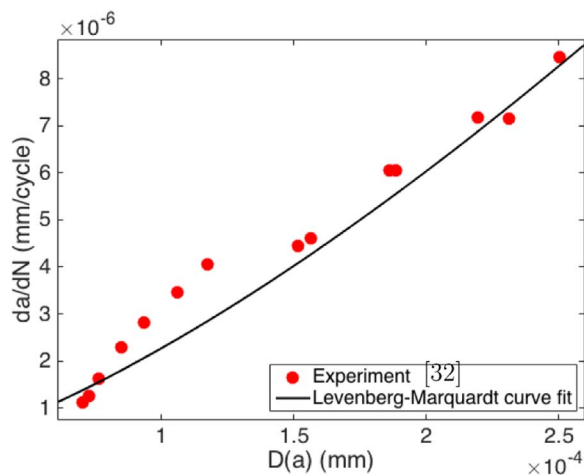
Fig. 10. Determining the relationship between the crack growth rate and the crack tip sliding displacement ($D(a)$).

Table 3
Schmid factors of the slip planes in the first and second grains.

Variable	Value	Unit	Reference
m_1	0.485		[35]
m_2	0.031		[35]
ΔK_{gb}	3.4	$MPa\sqrt{m}$	[35]

Table 3, to model the effect of the grain boundary. This critical stress intensity factor is the minimum value that the stress in front of the plastic tip has to reach in order to initiate a crack in the adjacent grain.

According to Marx et al. [32], there is only one class of slip system that is active in this FCC alloy ({111} < 110>). Thus, the friction stress (τ_{fail}) should be constant for this class of slip system. The applied stress changes from one slip system to another depending on the Schmid factor values. However, as in [32], instead of changing the applied stress across the grains, we use a stress transformation (Eq. (4.1)) to change the friction stress value from one grain to another.

$$\tau_{fail}^2 = \frac{1}{2}\sigma(1 - R)(m_1 - m_2) + \tau_{fail} \qquad (4.1)$$

Here, τ_{fail}^2 is the friction stress in the second grain, which is adjacent to the notched grain.

In Fig. 11, we use the calibrated parameters (τ_{fail}, h_s, and n) and the equations mentioned in Sections 2 and 3 to predict the microstructurally short fatigue crack growth across two grains. The crack
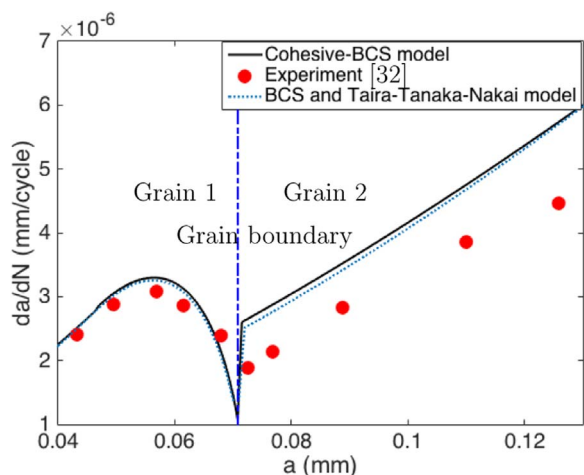
Fig. 11. Microstructurally short fatigue crack growth across a grain boundary.

initiates at a notch that is 30 μm from the grain boundary. Initially, in Grain 1, the equations derived in Section 2.2 are solved to calculate the crack tip sliding displacement. When the plastic zone in front of the crack tip reaches the grain boundary, we use the equations derived in Section 2.3 to calculate the crack tip sliding displacement. In Grain 1, when the crack growth rate is at a maximum, the plastic zone has reached the grain boundary. At this point, the crack stress at the plastic tip is lower than the critical stress required to cross the grain boundary. This causes the crack tip sliding displacement to reduce. This is shown in Fig. 11 by the decline in the crack growth rate as the crack approaches the grain boundary. As the crack tip approaches the grain boundary, the crack stress in front of the plastic tip is increasing due to the increase in the number of the dislocations that are piling up; at some point, it becomes greater than the value of the critical stress determined from the grain boundary critical stress intensity factor (ΔK_{gb}). This causes the most favorable slip system in Grain 2 to activate and the plastic zone to spread within the grain. In Fig. 11, we have plotted the results from both the BCS and Taira-Tanaka-Nakai models as well as our Cohesive-BCS model. The values of the parameters used in the BCS and Taira-Tanaka-Nakai models (, and n) are mentioned in Marx et al. [32]. Thus, as seen in Fig. 11, we have replaced the slip irreversibility parameter λ associated with the BCS and Taira-Tanaka-Nakai models with our Cohesive-BCS model parameter h_s and produced similar results for the microstructurally short fatigue crack growth across two grains. The parameter λ (Eq. (3.3)) cannot be determined from a lower scale simulation; rather, it is fitted to experimental data obtained from prior works [35]. However, the cohesive parameter h_s can be found from a lower scale simulation. Thus, it can be used to replace the fitting parameter λ from the formulation (Fig. 11). We would like to emphasize that the exponential cohesive law (Fig. 3) used in the present model is fully reversible; however, our formulation can also be used in conjunction with irreversible cohesive laws [38,39]. The addition of the variable λ would improve our fit, but it is not pursued in order to emphasize the effect of the cohesive parameter h_s.

5. Conclusion

This paper outlines the main features of a new dislocation theory-based cohesive model. We have combined the original Bilby-Cottrell-Swinden theory with cohesive theory to simulate microstructurally short fatigue crack growth. The key contribution of this paper is the ability to incorporate cohesive parameters that are obtainable from lower scale simulations (such as MD) into a higher length scale model based on dislocation interaction with microstructural features. To test the accuracy of our new formulation, we have compared our model with the original formulation and shown that our formulation reduces to the original formulation under a certain condition. We have also utilized our new formulation to predict microstructurally short fatigue crack growth across two grains in a Ni-based CMSX-4 alloy. The advantage of our method over the original formulation is that we have replaced one of the fatigue calibration parameters used in the original formulation with an energy-based cohesive parameter. The computational results show good correlation between the CMSX-4 experimental data and our model. We have also compared the Bilby-Cottrell-Swinden theory results with those of our formulation. In the near future, we plan to adapt the capabilities of this new formulation within our recent finite element model for fatigue failure [40].

Acknowledgments

Appendix A. Bounded solution with a cohesive zone

The cohesive zone equation is given by Eq. (2.2):

$$\ln(\tau_{fail}) - \ln(\tau_f(x)) = h_s \int_x^c B(x)dx, \quad a < |x| < c \tag{A.1}$$

The dislocation density equation for the bounded case is

$$B(x) = -\frac{2\alpha\sqrt{c^2 - x^2}}{\pi G} \int_{-c}^c \frac{\tau(x')}{(x - x')\sqrt{c^2 - x'^2}}dx', \quad -c < x < c \tag{A.2}$$

where the plastic zone size is calculated from the bounded condition for the dislocation density, which is given by Eq. (1.5):

$$\int_{-c}^c \frac{\tau(x)}{\sqrt{c^2 - x^2}}dx = 0 \tag{A.3}$$

The second condition on c (Eq. (1.6)) is satisfied by the symmetry of the stress field, $\tau(x)$.

The stress function is

$$\tau(x) = \begin{cases} \tau_f(x) - \tau_A, & a < |x| < c \\ -\tau_A, & |x| < a \end{cases} \tag{A.4}$$

Putting the above stress function, $\tau(x)$, into Eq. (A.3) gives

$$\int_a^c \frac{\tau(x)}{\sqrt{c^2 - x^2}}dx = \frac{\pi\tau_A}{2} \tag{A.5}$$

Eq. (A.2) is put into the cohesive equation, Eq. (A.1), and the result is

$$\ln(\tau_f(x)) - \ln(\tau_{fail}) = \frac{2\alpha h_s}{\pi G} \int_{-c}^c \frac{\tau(x')}{\sqrt{c^2 - x'^2}} \underbrace{\left(\int_x^c \frac{\sqrt{c^2 - x^2}}{(x - x')}dx\right)}_{I_1(x,x')} dx', \quad a < |x| < c \tag{A.6}$$

$I_1(x, x')$ in the above equation can be simplified as

$$\begin{aligned}
I_1(x, x') &= \int_x^c \frac{\sqrt{c^2 - x^2}}{(x - x')}dx \\
&= \int_x^c \frac{c^2x' + c^2x - x'x - x^3}{(x^2 - x'^2)\sqrt{c^2 - x^2}}dx \\
&= \frac{\sqrt{c^2 - x'^2}}{2} \ln\left|\frac{x\sqrt{c^2 - x'^2} + x'\sqrt{c^2 - x^2}}{x\sqrt{c^2 - x'^2} - x'\sqrt{c^2 - x^2}}\right| \\
&\quad + \frac{\sqrt{c^2 - x'^2}}{2} \ln\left|\frac{\sqrt{c^2 - x'^2} + \sqrt{c^2 - x^2}}{\sqrt{c^2 - x'^2} - \sqrt{c^2 - x^2}}\right| \\
&\quad - \sqrt{c^2 - x^2} - x'\left(\frac{\pi}{2} - \arcsin\frac{x}{c}\right)
\end{aligned} \tag{A.7}$$

Putting the simplified expression for $I_1(x, x')$ back into Eq. (A.6) gives

$$\ln(\tau_f(x)) - \ln(\tau_{fail}) = \frac{2\alpha h_s}{\pi G} \int_{-c}^c \left[\ln\left|\frac{x\sqrt{c^2 - x'^2} + x'\sqrt{c^2 - x^2}}{x\sqrt{c^2 - x'^2} - x'\sqrt{c^2 - x^2}}\right| + \frac{\sqrt{c^2 - x'^2}}{2} \ln\left|\frac{\sqrt{c^2 - x'^2} + \sqrt{c^2 - x^2}}{\sqrt{c^2 - x'^2} - \sqrt{c^2 - x^2}}\right| - \sqrt{c^2 - x^2} - x'\left(\frac{\pi}{2} - \arcsin\frac{x}{c}\right)\right]\tau(x')dx' \tag{A.8}$$

Utilizing the symmetry of the stress field (Eq. (1.6)) and Eqs. (A.4) and (A.5) in the above equation simplifies the above expression to

$$\ln(\tau_f(x)) = \frac{2h_s\alpha}{\pi G}\left(\int_a^c \tau_f(x')I_b(x, x')dx'\right) + \ln(\tau_{fail}), \quad a < |x| < c \tag{A.9}$$

Here,

$$I_b(x, x') = \ln\left|\frac{x\sqrt{c^2 - x'^2} + x'\sqrt{c^2 - x^2}}{x\sqrt{c^2 - x'^2} - x'\sqrt{c^2 - x^2}}\right| + \ln\left|\frac{\sqrt{c^2 - x'^2} + \sqrt{c^2 - x^2}}{\sqrt{c^2 - x'^2} - \sqrt{c^2 - x^2}}\right| - 2\frac{\sqrt{c^2 - x^2}}{\sqrt{c^2 - x'^2}}$$

Appendix B. Unbounded solution with a cohesive zone

Again, the cohesive zone equation is given by Eq. (2.2):

$$\ln(\tau_{fail}) - \ln(\tau_f(x)) = h_s \int_x^c B(x)dx, \quad a < |x| < c \tag{B.1}$$

The dislocation density equation for the unbounded case is

$$B(x) = -\frac{2\alpha\sqrt{c^2 - x^2}}{\pi G} \int_{-c}^{c} \frac{\tau(x')}{(x - x')\sqrt{c^2 - x'^2}} dx' - \frac{2\alpha}{\pi G} \frac{x}{\sqrt{c^2 - x^2}} \int_{-c}^{c} \frac{\tau(x')}{\sqrt{c^2 - x'^2}} dx' \quad, -c < x < c$$

(B.2)

The stress function is

$$\tau(x) = \begin{cases} \tau_f(x) - \tau_A, & a < |x| < c \\ -\tau_A, & |x| < a \end{cases}$$

(B.3)

The dislocation density equation (Eq. (B.2)) is put into the cohesive zone equation (Eq. (B.1)), resulting in

$$\ln(\tau_f(x)) - \ln(\tau_{fail}) = \frac{2\alpha h_s}{\pi G} \int_{-c}^{c} \frac{\tau(x')}{\sqrt{c^2 - x'^2}} \underbrace{\left(\int_{x}^{c} \frac{\sqrt{c^2 - x^2}}{(x - x')} dx \right)}_{I_1(x,x')} dx' + \frac{2\alpha h_s}{\pi G} \sqrt{c^2 - x^2} \int_{-c}^{c} \frac{\tau(x')}{\sqrt{c^2 - x'^2}} dx', \quad a < |x| < c$$

(B.4)

We can use $I_1(x, x')$ (Eq. (A.7)) from Appendix A in Eq. (B.4) to get

$$\ln(\tau_f(x)) - \ln(\tau_{fail}) = \frac{2\alpha h_s}{\pi G} \int_{-c}^{c} \tau(x') \left[\ln \left| \frac{x\sqrt{c^2 - x'^2} + x'\sqrt{c^2 - x^2}}{x\sqrt{c^2 - x'^2} - x'\sqrt{c^2 - x^2}} \right| + \ln \left| \frac{\sqrt{c^2 - x'^2} + \sqrt{c^2 - x^2}}{\sqrt{c^2 - x'^2} - \sqrt{c^2 - x^2}} \right| \right] dx' - \frac{2\alpha h_s}{\pi G} \int_{-c}^{c} \left(\frac{\pi}{2} - \arcsin\frac{x}{c} \right) \frac{x'\tau(x')}{\sqrt{c^2 - x'^2}} dx',$$

$$a < |x| < c$$

(B.5)

Finally, we can use the stress function (Eq. (B.3)) in the above expression to get

$$\ln(\tau_f(x)) = \frac{2h_s\alpha}{\pi G} \left(\int_{a}^{c} \tau_f(x') I_u(x, x') dx' \right) - \frac{2h_s\alpha\tau_A}{G} \sqrt{c^2 - x^2} + \ln(\tau_{fail}), a < |x| < c$$

(B.6)

Here, $I_u(x, x')$ is given by

$$I_u(x, x') = \ln \left| \frac{x\sqrt{c^2 - x'^2} + x'\sqrt{c^2 - x^2}}{x\sqrt{c^2 - x'^2} - x'\sqrt{c^2 - x^2}} \right| + \ln \left| \frac{\sqrt{c^2 - x'^2} + \sqrt{c^2 - x^2}}{\sqrt{c^2 - x'^2} - \sqrt{c^2 - x^2}} \right| - 2 \left(\frac{\pi}{2} - \arcsin\frac{x}{c} \right) \frac{x'}{\sqrt{c^2 - x'^2}}$$

Appendix C. A piecewise polynomial collocation method

The kernels of the integrands of Eqs. (A.6) and (B.6) are singular when $x = x'$ as well as at the domain boundaries ($x, x' = a, c$). Thus, to solve these types of weakly singular Fredholm equations, we make use of polynomial splines with a graded mesh [34].

Using the method described in Brunner et al. [34], we split our domain ($a < |x| < c$) in half. Let $a = x_0 < x_1 < .... < x_N = \frac{c+a}{2}$ be the partition points for the first half of the domain. The partition points for the second half of the domain ($x_{N+1}, ..., x_{2N}$) are obtained by reflecting the partition points of the first half about $x_N = \frac{c+a}{2}$. The mesh nodes for the first half of the domain are determined by

$$x_j = a + \left(\frac{j}{N} \right)^r \left(\frac{c - a}{2} \right), \quad j = 0, 1, 2, ..., N$$

and the points of the second half are calculated by

$$x_{j+N} = c + a - x_{N-j}, \quad j = 1, 2, 3, ..., N$$

For every subinterval ($[x_j, x_{j+1}]$, $j = 1, 2, ..., 2N$), we choose $m = 2$ collocation points, which are given by

$$\xi_{ji} = x_j + \frac{\eta_i + 1}{2}(x_{j+1} - x_j), \quad i = 1, 2$$

(C.1)

Here, η_1 and η_2 are the gauss quadrature points that satisfy the following condition:

$$-1 \leq \eta_1 \leq \eta_2 \leq +1$$

In this paper, we use $\eta_1 = -\frac{1}{\sqrt{3}}$ and $\eta_2 = \frac{1}{\sqrt{3}}$.

We assume that the piecewise polynomial interpolation τ_{fN}: $[a, c]$ can be used instead of a continuous function τ_f in the weakly singular equations. On every subinterval $[x_{j-1}, x_j]$, ($j = 1, ..., 2N$), τ_{fN} is a polynomial of degree 1 and interpolates τ_f at the points ξ_{j1} and ξ_{j2}.

$$\tau_{fN}(\xi_{ji}) = \tau_f(\xi_{ji}), \quad i = 1, 2; \quad j = 1, ..., 2N$$

Thus, this interpolation function is independently defined on each subinterval $[x_{j-1}, x_j]$, ($j = 1, ..., 2N$) and may be discontinuous at the interior grid points $x = x_j$, ($j = 1, ..., 2N - 1$). The interpolation function τ_{fN} in the interval $[x_{j-1}, x_j]$, ($j = 1, ..., 2N$) is represented as

$$\tau_{fN}(x) = \sum_{i=1}^{2} s_{ji} \phi_{ji}(x), \quad x \in [x_{j-1}, x_j]$$

where $\phi_{ji}(x)$, $x \in [x_{j-1}, x_j]$ is a polynomial of degree $m - 1$, such that

$$\phi_{ji}(\xi_{jk}) = \begin{cases} 1, & if \quad k = i \\ 0, & if \quad k \neq i \end{cases}, \quad k = 1, ..., m$$

In this paper, the approximate solution τ_{fN} within the interval $[x_{j-1}, x_j]$, ($j = 1, ..., 2N$) is represented as

$$\tau_{fN}(x) = s_{j1} \frac{\xi_{j2} - x}{\xi_{j2} - \xi_{j1}} + s_{j2} \frac{x - \xi_{j1}}{\xi_{j2} - \xi_{j1}}, \quad x_{j-1} \leq x \leq x_j$$

(C.2)

Here, ξ_{j1} and ξ_{j2} are determined from Eq. (C.1), and the coefficients s_{j1} and s_{j2} are the unknown variables.

Thus, for the condition in which the crack and the associated plastic zone are completely inside a grain, Eqs. (A.5) and (A.9) are discretized as

$$\sum_{j=1}^{2N} \sum_{i=1}^{2} \left[\ln(s_{ji}) - \ln(\tau_{fail}) = \frac{2h_s \alpha}{\pi G} \left\{ \sum_{l=1}^{2N} \int_{x_{l-1}}^{x_l} \left(s_{l1} \frac{\xi_{l2} - x'}{\xi_{l2} - \xi_{l1}} + s_{l2} \frac{x' - \xi_{l1}}{\xi_{l2} - \xi_{l1}} \right) I_b(x, x') dx' \right\} \right] \tag{C.3}$$

$$\sum_{l=1}^{2N} \int_{x_{l-1}}^{x_l} \left(s_{l1} \frac{\xi_{l2} - x'}{\xi_{l2} - \xi_{l1}} + s_{l2} \frac{x' - \xi_{l1}}{\xi_{l2} - \xi_{l1}} \right) \frac{1}{\sqrt{c^2 - x^2}} dx = \frac{\pi \tau_A}{2} \tag{C.4}$$

These are coupled nonlinear equations with unknown variables s_{ji}, $j = 1, ..., 2N$, $i = 1, 2$ and c.

Similarly, for the condition in which the plastic zone in front of the crack tip has reached a grain boundary, Eq. (B.6) is discretized as

$$\sum_{j=1}^{2N} \sum_{i=1}^{2} \left[\ln(s_{ji}) - \ln(\tau_{fail}) + \frac{2h_s \alpha \tau_A}{G} \sqrt{c^2 - x^2} = \frac{2h_s \alpha}{\pi G} \left\{ \sum_{l=1}^{2N} \int_{x_{l-1}}^{x_l} \left(s_{l1} \frac{\xi_{l2} - x'}{\xi_{l2} - \xi_{l1}} + s_{l2} \frac{x' - \xi_{l1}}{\xi_{l2} - \xi_{l1}} \right) I_u(x, x') dx' \right\} \right] \tag{C.5}$$

These equations (Eqs. (C.3) and (C.5)) are solved for the unknown variables using the Newton-Raphson numerical scheme.

After solving Eq. (C.5), the unbounded dislocation density is determined from Eq. (B.2). The unbounded dislocation density is then used in Eq. (1.14) to find the stress in the adjacent grain at a distance r_0 from the grain boundary ($S(r_0)$), which is produced by the dislocations piling up at the grain boundary.

References

[1] H.-J. Christ, C.-P. Fritzen, P. Köster, Micromechanical modeling of short fatigue cracks, Curr. Opin. Solid State Mater. Sci. 18 (4) (2014) 205–211.

[2] J. Newman Jr, E.P. Phillips, R. Everett Jr, Fatigue analyses under constant-and variable-amplitude loading using small-crack theory, NASA TM 209329 (1999).

[3] J. Newman, E.P. Phillips, M. Swain, Fatigue-life prediction methodology using small-crack theory, Int. J. Fatigue 21 (2) (1999) 109–119.

[4] P. Hobson, The formulation of a crack growth equation for short cracks, Fatigue Fract. Eng. Mater. Struct. 5 (4) (1982) 323–327.

[5] B. Bilby, A. Cottrell, K. Swinden, The spread of plastic yield from a notch, Proc. R. Soc. Lond. A: Math., Phys. Eng. Sci. 272 (1350) (1963) 304–314.

[6] S. Taira, K. Tanaka, Y. Nakai, A model of crack-tip slip band blocked by grain boundary, Mech. Res. Commun. 5 (6) (1978) 375–381.

[7] K. Tanaka, Y. Akiniwa, Y. Nakai, R. Wei, Modelling of small fatigue crack growth interacting with grain boundary, Eng. Fract. Mech. 24 (6) (1986) 803–819.

[8] A. Navarro, E. Rios, A model for short fatigue crack propagation with an interpretation of the short-long crack transition, Fatigue Fract. Eng. Mater. Struct. 10 (2) (1987) 169–186.

[9] A. Navarro, E. De Los Rios, Short and long fatigue crack growth: a unified model, Philos. Mag. A 57 (1) (1988) 15–36.

[10] A. Navarro, E. Rios, A microstructurally-short fatigue crack growth equation, Fatigue Fract. Eng. Mater. Struct. 11 (5) (1988) 383–396.

[11] A. Navarro, E. De Los Rios, An alternative model of the blocking of dislocations at grain boundaries, Philos. Mag. A 57 (1) (1988) 37–42.

[12] C. Heinrich, V. Sundararaghavan, A method to predict fatigue crack initiation in metals using dislocation dynamics, in press, (2017).

[13] A. Head, N. Louat, The distribution of dislocations in linear arrays, Aust. J. Phys. 8 (1) (1955) 1–7.

[14] D. Dugdale, Yielding of steel sheets containing slits, J. Mech. Phys. Solids 8 (2) (1960) 100–104.

[15] G.I. Barenblatt, The mathematical theory of equilibrium cracks in brittle fracture, Adv. Appl. Mech. 7 (1) (1962) 55–129.

[16] J. Willis, A comparison of the fracture criteria of griffith and barenblatt, J. Mech. Phys. Solids 15 (3) (1967) 151–162.

[17] A. Hillerborg, M. Modéer, P.-E. Petersson, Analysis of crack formation and crack growth in concrete by means of fracture mechanics and finite elements, Cem. Concr. Res. 6 (6) (1976) 773–781.

[18] J. Planas, M. Elices, G. Guinea, F. Gómez, D. Cendón, I. Arbilla, Generalizations and specializations of cohesive crack models, Eng. Fract. Mech. 70 (14) (2003) 1759–1776.

[19] F. Gómez, M. Elices, F. Berto, P. Lazzarin, Fracture of u-notched specimens under mixed mode: experimental results and numerical predictions, Eng. Fract. Mech. 76 (2) (2009) 236–249.

[20] G.T. Camacho, M. Ortiz, Computational modelling of impact damage in brittle materials, Int. J. Solids Struct. 33 (20–22) (1996) 2899–2938.

[21] W. Knauss, Time dependent fracture and cohesive zones, Trans.-Am. Soc. Mech. Eng. J. Eng. Mater. Technol. 115 (1993) 262.

[22] D. A. Cendón, F. Berto, P. Lazzarin, M. Elices Calafat, The cohesive crack model applied to notched pmma specimens obeying a non linear behaviour under torsion loading, in: Key Engineering Materials, Vol. 577, Trans Tech Publications, 2014, pp. 49–52.

[23] A. Needleman, A continuum model for void nucleation by inclusion debonding, J. Appl. Mech. 54 (3) (1987) 525–531.

[24] M. Elices, G. Guinea, J. Gomez, J. Planas, The cohesive zone model: advantages, limitations and challenges, Eng. Fract. Mech. 69 (2) (2002) 137–163.

[25] A. Needleman, Some issues in cohesive surface modeling, Procedia IUTAM 10 (2014) 221–246.

[26] J. Weertman, Theory of fatigue crack growth based on a bcs crack theory with work hardening, Int. J. Fract. 9 (2) (1973) 125–131.

[27] N. Muskhelishvili, J. Radok, Singular Integral Equations: Boundary Problems of Functions Theory and Their Application to Mathematical Physics, P. Noordhoff, Netherland, 1953.

[28] A.J. Wilkinson, Modelling the effects of texture on the statistics of stage i fatigue crack growth, Philos. Mag. A 81 (4) (2001) 841–855.

[29] A. J. Wilkinson, Modelling the effects of microstructure and microtexture on the statistics of short fatigue crack growth, in: ICF10, Honolulu (USA) 2001, 2001.

[30] E.H. Glaessgen, E. Saether, D.R. Phillips, V. Yamakov, Multiscale modeling of grain-boundary fracture: cohesive zone models parameterized from atomistic simulations, in: Proceedings of the 47th AIAA/ASME/ASCE/AHS/ASC Structures, Structural Dynamics, and Materials Conference, 2006, pp. 1–4.

[31] S. Lee, V. Sundararaghavan, Calibration of nanocrystal grain boundary model based on polycrystal plasticity using molecular dynamics simulations, Int. J. Multiscale Comput. Eng. 8 (5) (2010) 509–522.

[32] M. Marx, W. Schaef, M. Welsch, The microstructure as crack initiation point and barrier against fatigue damaging, Int. J. Fatigue 41 (2012) 57–63.

[33] J. Weertman, Dislocation based fracture mechanics, World Scientific Publishing Co Inc., 5 Toh Tuck Link, Singapore, 596224, 1996.

[34] H. Brunner, A. Pedas, G. Vainikko, The piecewise polynomial collocation method for nonlinear weakly singular volterra equations, Math. Comput. Am. Math. Soc. 68 (227) (1999) 1079–1095.

[35] W. Schaef, M. Marx, A numerical description of short fatigue cracks interacting with grain boundaries, Acta Mater. 60 (5) (2012) 2425–2436.

[36] A. Sengupta, S. Putatunda, L. Bartosiewicz, J. Hangas, P. Nailos, M. Peputapeck, F. Alberts, Tensile behavior of a new single-crystal nickel-based superalloy (cmsx-4) at room and elevated temperatures, J. Mater. Eng. Perform. 3 (1) (1994) 73–81.

[37] MATLAB, version 9.1.0.441655 (R2016b), The MathWorks Inc., Natick, Massachusetts, 2016.

[38] A. Ural, V.R. Krishnan, K.D. Papoulia, A cohesive zone model for fatigue crack growth allowing for crack retardation, Int. J. Solids Struct. 46 (11) (2009) 2453–2462.

[39] S. Maiti, P.H. Geubelle, A cohesive model for fatigue failure of polymers, Eng. Fract. Mech. 72 (5) (2005) 691–708.

[40] S. Panwar, S. Sun, V. Sundararaghavan, Modeling fatigue failure using the variational multiscale method, Eng. Fract. Mech. 162 (2016) 290–308.